Medicon Engineering Themes
Volume 8 Issue 2 February 2025
Article Type: Research Article
ISSN: 2834-7218

Capillary Forces Computation on Dynamic Spreading of a Nanosuspension Droplet

Baiou Shi*, Viet Le and Siddharth Ravi

Penn State Erie, The Behrend College, Erie, PA 16563, USA

***Corresponding Author:** Baiou Shi, Penn State Erie, The Behrend College, Erie, PA 16563, USA.

Received: January 06, 2025; **Published:** January 23, 2025

DOI: 10.55162/MCET.08.261

Abstract

This study investigates the mechanism behind the dynamic spreading of liquid nano-droplets with suspended nanoparticles, focusing on the impact of nanoparticle size and interaction strength using molecular dynamics simulations. Building on our prior research with Pb-Cu wetting systems of identical chemistry that revealed distinct spreading behaviors, the current findings demonstrate that particle characteristics and interatomic potentials significantly affect the nanosuspension spreading process. The strength of the interaction between the particle and underlying substrate varies from the interatomic potential to test the dynamic spreading behavior of nanofluid droplets, to explore how it affects the wetting kinetics. Meanwhile, forces acting on suspended particles are directly computed from molecular dynamics simulations and compared with cases of different particle sizes. Mechanisms are discussed by correlating the force data with the contact line advancement, droplet morphology, and the observed pinning/depinning behavior.

Keywords: particle suspension; molecular dynamics; force computation

Introduction

The spreading and evaporation behavior of liquid droplets on solid surfaces has garnered significant interest due to its applications in photonics, microelectronics, and biotechnology [1]. Over the past two centuries, much research has focused on the spreading of pure liquids and the capillary forces that govern their motion across solid surfaces [2, 3]. However, when nanoparticles are introduced into nano-droplets, their spreading dynamics differ significantly from those of pure liquids. The complex interactions among particles, the liquid medium, and the substrate introduce new challenges, making the spreading behavior less predictable. These phenomena have practical implications, as nanoparticle suspensions play a crucial role in processes such as drug delivery, oil recovery, and semiconductor production [4-6]. The advent of advanced nanotechnology allows the incorporation of engineered nanoparticles into liquid droplets to modify their spreading and evaporation behaviors, which has led to growing interest in understanding how nano-suspensions influence these processes.

Research has shown that studying the distribution of nanoparticles in suspensions can enable low-cost methods for creating nanoparticle arrays with specific properties—such as electrical, optical, and structural functionalities—critical for semiconductor applications [7]. Additionally, solvent evaporation, a pathway for particle self-assembly, can provide insights into low-cost, rapid diagnostic techniques by analyzing strain patterns left by drying biological fluids, such as blood or saliva [8-10]. Using confocal laser microscopy, Dr. Kim and colleagues visualized individual colloidal particles with varying sizes and volume fractions, identifying how these factors influence crack generation. This work offers potential solutions for crack prevention in industrial applications like painting and inkjet printing [11]. Similarly, studies of the "coffee-ring effect" demonstrated that different initial particle volume fractions

lead to variations in colloidal ring-stain formation [12]. Dr. Ghosh further explored the effects of liquid polarity on contact line dynamics, showing that altering liquid polarity decreases contact line velocity [13]. People found that nanoparticles affect interfacial regions and wettability, particularly near the contact line, where they influence fluid flow, liquid front velocity, advancing contact angle, and droplet morphology [14]. Dr. Weon recently proposed an expression for the forces acting on particles near the contact line, predicting the critical packing fraction for pinning and validating these findings experimentally [15]. Additional studies have developed force balance models to understand these mechanisms [16]. Despite extensive experimental and theoretical investigations, quantitative evidence on the role of nano-suspension particles in wetting and drying processes remains limited.

Although numerous experimental and theoretical studies have explored nano-suspension spreading, a detailed atomistic understanding of nanoparticle effects and the associated forces during the spreading process remains lacking. The mechanisms by which these forces evolve and influence spreading, as well as the role of suspension particles, are not well understood. Given the nanoscale length and time involved, molecular dynamics (MD) simulations provide an ideal approach for investigating these phenomena. MD simulations offer detailed insights into interfacial thermodynamics and fluid-particle mechanics, helping to clarify the driving forces behind nano-suspension wetting and bridging particle behavior with wetting kinetics.

This work builds on our recent study of nano-suspension wetting using MD simulations. The primary objective is to examine how nanoparticle size and interaction strength influences wetting kinetics and capillary forces. By systematically varying the interaction strength between particles and the substrate through interatomic potentials, we explore their impact on dynamic spreading behavior. Forces acting on suspended particles are directly calculated from MD simulations and analyzed for different particle sizes. Mechanisms are elucidated by correlating force data with contact line motion, droplet morphology, and observed pinning or depinning behavior, contributing to a deeper understanding of nanoscale wetting dynamics.

Procedures

Because of the relative immiscibility between Pb and Cu, thus the Cu particles are stable in the liquid and do not dissolve during spreading, Pb(liquid)/Cu(solid) system is investigated in this paper as a reasonable model to explore the nanoparticle suspensions. Meanwhile, there is a significant difference in the droplet morphology and spreading rate for pure Pb(l) drops spreading on Cu(001) versus Cu(111), despite identical chemistry. From previous work, Lower θ_{adv} and higher contact line velocity is observed on Cu(111). This system has been explored via both experiments and simulations. Especially the previous MD simulation results showed good agreement with experimental observations. [17] At 700K, drops adopt partial wetting on the two Cu surfaces and the final contact angles are θ_0 = 30° for Cu(001) and θ_0 = 20° for Cu(111). Furthermore, from our previous study on the nanosuspension droplet spreading of this system, self-pinning is observed for low θ_{adv} whereas depinning for high θ_{adv}. Therefore, this Pb(l)/Cu(s) system shows its extremely high potential to dig into it.

To model the metallic system of Pb (liquid) drops with suspended Cu (solid) nanoparticles spreading on Cu solid surfaces, we used classical MD simulations employing the embedded atom method (EAM) to achieve the goals. [18] EAM is an alternative simple but rather realistic approach to describe the metallic cohesion for its embedding function dependent on the local electron density while pair potentials cannot provide an adequate description of metallic systems. Employing EAM allows us to account for the dependence of the strength of individual bonds on the local environment which is important for the simulation of surfaces and defects. Moreover, EAM potentials have been proven to describe some metallic systems with very high accuracy, compared to experimental results and density functional theory-based calculations.

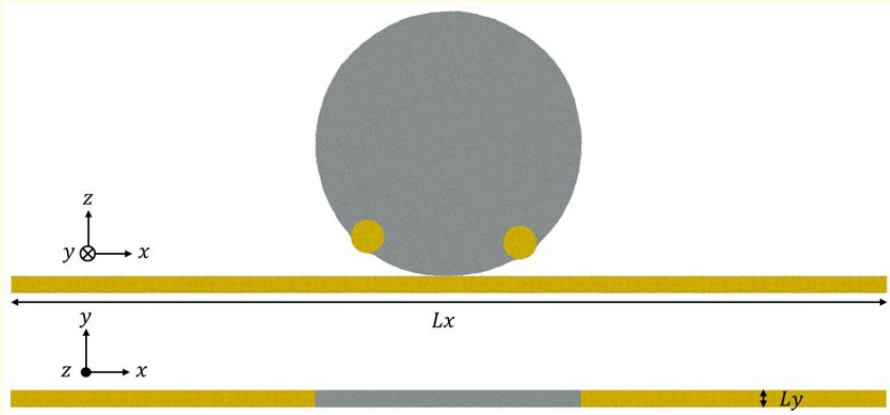

Figure 1: Front and top views of initial simulation configuration at $t = 0$ (Pb atoms are gray; Cu atoms are yellow). The image is for a R_0 = 42 nm drop with two Cu particles in contact with the Cu (001) surface, with the spreading direction along the x-axis and the free surface normal along the z-axis, and the cylindrical axes of both the droplet and particles are aligned along the y-axis. The periodic repeat lengths of the simulation cells are set to L_x = 300 nm and L_y = 5 nm.

In this paper, the specific EAM interatomic potential for the Pb-Cu system we employed is formulated by Hoyt, etc. [19]. In this model, we employed the previously derived EAM potentials for pure Pb and Cu to describe the embedding and density functions for pure Pb, Cu, and the Pb-Pb, Cu-Cu pair interaction term. [20, 21] Meanwhile, The Pb-Cu cross term is optimized using a fitting procedure based on comparing the computed heat of mixing of Pb-Cu liquids and the evaluated phase diagram with experimental results. LAMMPS was employed for all simulations and isothermal wetting simulations for $T = 700K$ were explored in all cases; the interaction model typically exhibits high surface tension and low viscosity.

Fig. 1 shows two views of a typical dilute limit simulation configuration at time zero. Fully three-dimensional simulations were employed throughout; however, to reduce the spreading geometry to two dimensions, liquid cylinders were brought into contact with solid surfaces where the length of the cylinder along its axis (i.e., in the y direction) was identical to the periodic dimension of the simulation cell along y (the same was true for the solid surface). Results were averaged along *y* to collapse spreading analyses into the *xz* plane. Like what was done with the liquid drop, the two suspended nanoparticles are also cylinders. Both Cu substrates modeled were subject to periodic boundary conditions in x and y with the periodic repeat length of the simulation cells $L_x \sim 300\ nm$ and $L_y \sim 5\ nm$. Substrate L_x was chosen to permit significant droplet spreading without reaching the edge of the simulation cell while L_y was chosen as ten times the EAM interaction model's cutoff distance without too much interaction. Additionally, seven different particle sizes were modeled with particle radius of 2.6 *nm*, 3.4 *nm*, 4.2 *nm*, 5 *nm*, 5.8 *nm*, 6.6 *nm*, and 7.5 *nm*. The initial droplet radius was R_0 = 42 nm in all cases studied here.

As the first step in model development, Cu(001) substrates were equilibrated at the zero-pressure lattice constant, with their crystallographic direction aligned along the z-axis. After equilibration, periodic boundary conditions along the z-axis were removed, creating two free surfaces on each substrate. Similarly, 3D periodic slabs of liquid Pb were equilibrated at zero-pressure density. Cylindrical droplets were then extracted from the liquid slabs and re-equilibrated in free space. To insert nanoparticles, a cylindrical region of liquid atoms was removed from the droplet, and the cylindrical particle was inserted at the specified location. Following particle insertion, the nanosuspension droplets were re-equilibrated. These equilibrated droplets were then prepared for wetting simulations by positioning them above the Cu(001) substrate along the positive z-direction, with the initial separation distance set to the equilibrium value observed in planar solid/liquid interface simulations. The final wetting models, incorporating nanoparticles of varying sizes,

were established for further simulation studies to analyze dynamic wetting behavior.

Results and Discussion

In our recently published work in Physical Review E [21], we have explored pinning and depinning events at the atomistic scale during the spreading of liquid droplets containing suspended nanoparticles. In our spreading simulations, cylindrical Pb droplets containing cylindrical Cu nanoparticles were modeled on two different Cu surfaces: Cu(001) and Cu(111). For identical chemistry, varying advancing contact angles θ_{adv} were exhibited on these substrate surfaces. We found that self-pinning occurred for lower θ_{adv} while depinning was observed for higher θ_{adv}. Meanwhile, the particle loading effect was also investigated and the spreading behavior was affected by whether particles are being entrained to the advancing contact line, which depends on particle's initial position within the drop at time zero. In this paper, as a continuum study on the particle suspension behavior, we dig into more spreading scenarios by varying particle size, by doing so the mechanism behind the self-pinning could be studied.

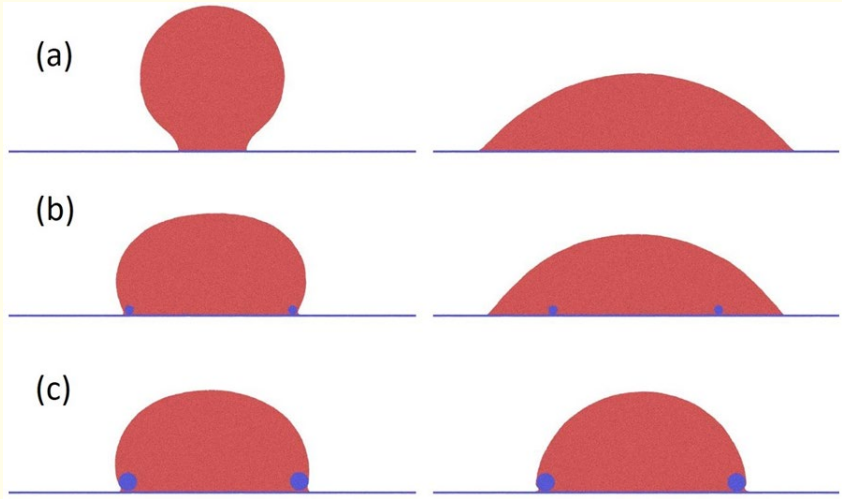

Figure 2: Simulation snapshots of systems at t = 2 ns & t = 6 ns: (a) pure droplet wetting Cu(001); (b) droplet wetting with two particles (radius = 2.6 nm) Cu(001); (c) droplet wetting with two particles (radius = 5.0 nm) Cu(001).

Figure 2 shows the time evolution for three different scenarios of droplet spreading: pure spreading, de-pinning, and pinning, respectively. It indicates the effect of nanoparticles during the wetting process; the particles inside the droplet would promote the spreading speed at the early stage but slow it significantly at the late time. Meanwhile, case (b) shows that the particles would leave behind the contact line at a specific time point when the particle size is small. And this is so-called "de-pinning". Besides, case (c), which is "pinning", provided a clear view of how the spreading processes are affected by particles. The particles would stick with the contact line while the contact line advanced and even prevent it from moving.

To characterize spreading kinetics the extent of wetting versus time, $x(t)$ for all systems is shown in Fig. 3. Data was obtained by measuring the distance from the edge of the droplet to the center of the drop. Moreover, to make sure the indictable of droplet spreading kinetic data and to avoid the precursor film advancement, the edge of the third layer, the layer above the two-layer precursor film, was considered as the edge of the droplet for all systems. Because of the symmetry of the simulation, events for both contact lines were considered identical for all cases investigated here. Therefore, the data used to produce $x(t)$ plots in each system were averaged for the two contact lines.

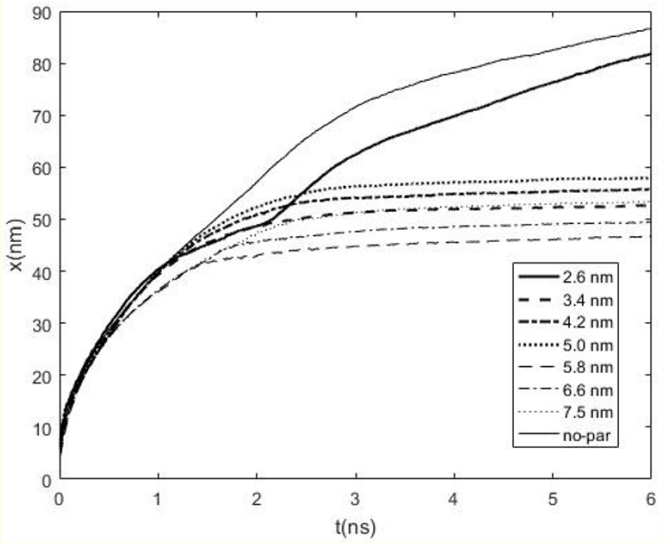

Figure 3: Extent of droplet spread in x versus time t. Data are presented for Pb droplets wetting on Cu (001) substrate for varying particle size: Radius = 2.6 nm, 3.4 nm, 4.2 nm, 5.0 nm, 5.8 nm, 6.6 nm, 7.5 nm, and no particles.

Examining the plots in Fig. 3, it can be seen that both contact lines with particles inside advanced nearer than the pure spreading contact line. The depinning behaviors could be easily observed during the spreading process from $t \sim 1$ ns to $t \sim 3$ ns for the case with a 2.6 nm radius particle inside. Moreover, it is not hard to notice, even the particle size increased a little bit, from a 2.6 nm radius to 3.4 nm, droplet pinning could be observed, which can be seen in the kinetic curves shown in this figure. Comparing the curves of 3.4 nm, 4.2 nm, and 5.0 nm, particle size effects on contact line advancing could be obtained, larger particle size leads to farther liquid front. To examine this, three more scenarios were investigated. However, while larger particles were inserted into the droplet, the phenomenon was observed that the liquid could not spread out through the space between these two particles but blow up to a higher region. This indicates that the initial position of droplet particles may affect the spreading process. And this Siphon-like phenomenon might provide another view of how to control colloidal fluid spreading, which we might dig into in later research. Therefore, the initial positions have changed in the next three cases (5.8 nm, 6.6 nm, and 7.5 nm) to achieve the goal.

A similar trend could be observed by comparing these curves, the distance between the center of the droplet and the edge of the droplet would be increased as the particle size increases. It could be noticed that the curves for these cases are almost the same at the early stage, which shows the initial velocity of each case should be similar. Therefore, the larger particle should have bigger kinetic energy which needs a longer spreading distance to prevent it from moving. However, the capillary forces that act on the suspended particles are still needed to computed to understand the mechanism.

Fig. 4 shows a simulation snapshot taken at t = 6 ns where the contact line is pinned by the outermost Cu particle on Cu(001) substrate. The region highlighted in the zoom-in reveals details about the atomic arrangement at the interface between the Cu particle and the underlying Cu substrate. Careful examination of the particle-substrate interface shows that a sufficient number of Cu-Cu bonds have formed there to partially eliminate the liquid film between particle and substrate. This halts particle advancement, leading to contact line pinning.

In order to compute the capillary forces, the systems were supposed to spatially divide into 6 different regions like our previous PRE paper. [21] Nonetheless, a very complicated region was observed in each pinning case, some liquid atoms were trapped in the region between the particle and solid surface. Therefore, the capillary force liquid acts on the particle should be quite different, which means

the previous separation is not feasible for this situation. By measuring the density along the x direction, the length of this special region was found, which is almost equal to 0.8 of the particle radius. Based on this, the systems were spatially divided into 9 regions with the ratio 3:4:3 along both x and z directions, which can be seen in Fig. 5. Thus, the separate groups were formed from all the liquid atoms in each of the regions indicated. Due to atoms transporting into and out of the region with time, the liquid atom group information was updated frequently. Also defining the particle atoms as a distinct group is necessary to allow LAMMPS to compute the net force acts on the particle due to all the liquid atoms in each spatial group. Though, in this research, the force calculated was the force that liquid atoms exert on the particle, Newton's third law gives us that this must be the same force that the particle atoms exert on the liquid in that region. Moreover, the forces were averaged sufficiently to reduce the error in the calculation to order 0.1 nN.

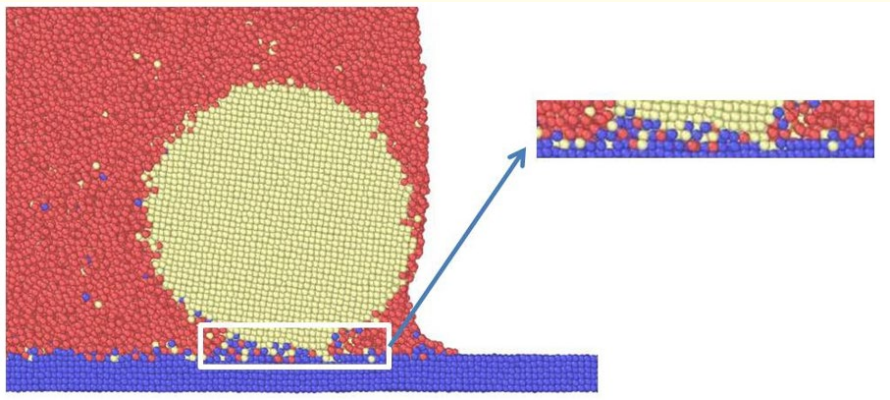

Figure 4: Simulation snapshot and zoom-in of Pb droplet wetting with two Cu particles (radius = 4.2 nm) on Cu(001) at t = 6 ns.

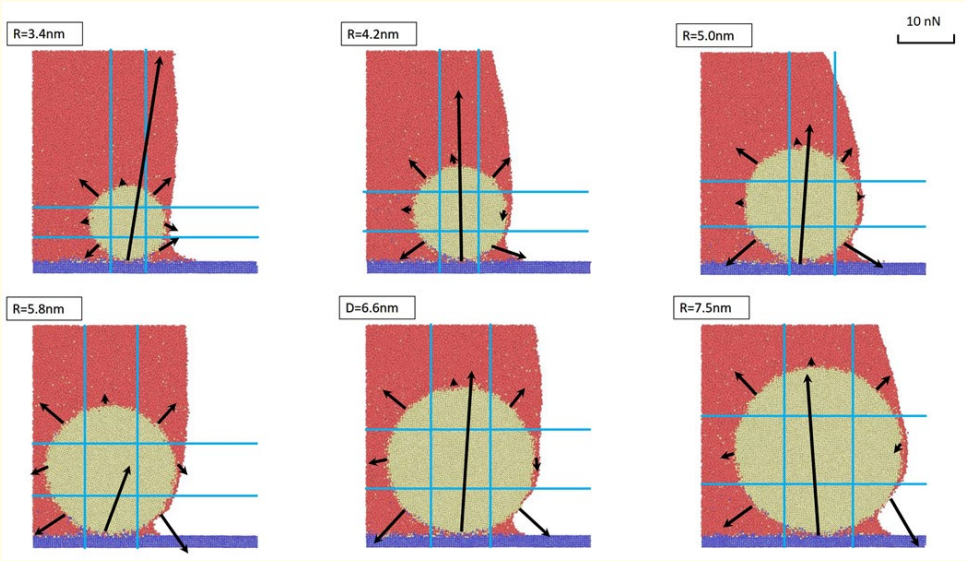

Figure 5: Capillary forces of particles act on the liquid atoms. Force contributions are categorized according to the location of liquid atoms within the system, as indicated by the horizontal and vertical blue dividing lines.

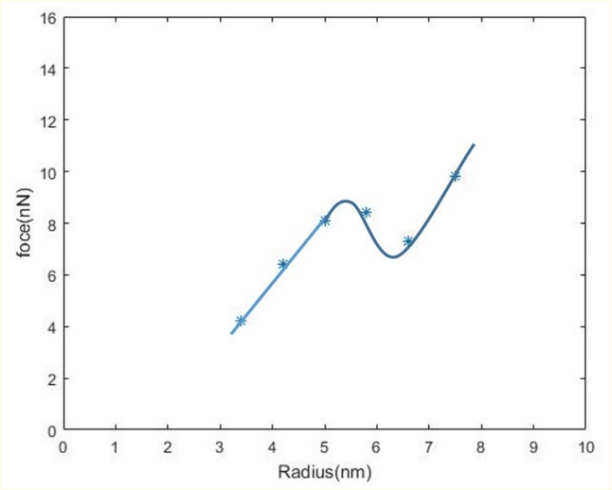

Figure 6: The relationship between the computed capillary force of the bottom-right region and particle size in radius.

By observing and comparing forces acting due to different regions for these six scenarios, the force of the bottom-right region might be the force most directly associated with the pinning of the liquid front and it affects the pinning behavior most. Therefore, data of this specific region's forces were collected and plotted in Fig. 6. Based on the data calculated by LAMMPS, the magnitudes of the capillary forces of the bottom-right liquid region acting on the particles are 4.2 nN, 6.4 nN, 8.1 nN, 8.4 nN, 7.3 nN, and 9.8 nN, respectively for particle radius of 3.4 nm, 4.2 nm, 5.0 nm, 5.8 nm, 6.6 nm, and 7.5 nm. As expected, the force increases with particle size in general, except for one data point.

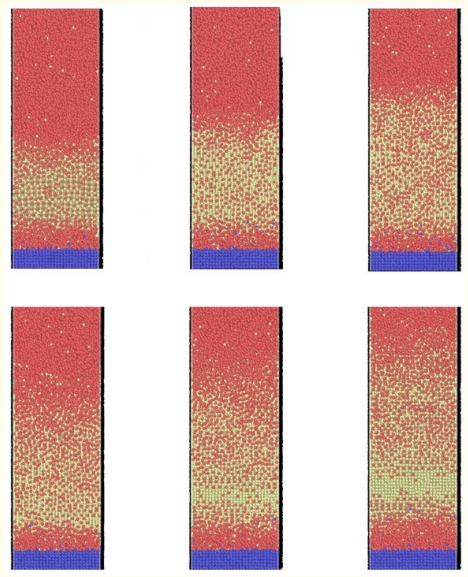

Figure 7: Simulation y-z plane view zoom-in snapshots of systems at t = 6 ns for varying particle size: Radius = 3.4 nm, 4.2 nm, 5.0 nm, 5.8 nm, 6.6 nm, and 7.5 nm.

For the first three data points, a reasonable linear fit could be obtained. Combining the idea Dr. Weon proposed in his paper [15] (and similar to what other authors have advanced) and considering the cylindrical particle geometry, we assumed a slope given by $2\pi\gamma\cos\theta$, which γ is the liquid-vapor surface tension for this system. Then θ was allowed to vary and found that the best fit was obtained for it equals 50 degrees. This is in remarkably good agreement with the equilibrium contact angle for this solid/liquid combo. However, the next three data points show a unique trend: the force decreases after a slight increase, and then it increases tremendously.

To investigate this more, Fig. 7 was obtained to help understand the mechanism. Capillary forces were calculated by adding all forces between the solid atoms and liquid atoms. Fig. 7 provides detailed insights into the behavior of capillary forces as particle size varies, depicted through simulation snapshots at 6 ns. For smaller particles, with radii ranging from 3.4 nm to 5.0 nm, the liquid atoms uniformly distribute on the particle surface, resulting in an increase in the interaction area proportional to the particle size. This uniformity explains the observed linear relationship between the capillary force and particle size for these smaller cases. However, when the particle size reaches 5.8 nm, the distribution changes due to altered surface tension and geometry, leading to fewer liquid atoms at the bottom of the interaction area. This reduction results in a non-linear response, where the capillary force increases only slightly. As the particle radius grows to 6.6 nm, a distinct barrier appears, characterized by a region with no acting interaction forces. This barrier disrupts the expected increase in capillary force, resulting in a decrease at this point. When the particle size continues to increase (7.5 nm), the interaction area shifts, trapping more atoms in the right-bottom region of the system. Although the empty space continues to expand, its rate of increase becomes slower compared to the size growth, causing the capillary force to rise once again. This behavior between 5.8 nm and 7.5 nm is defined as the "transition region," where the growth rate of the interaction area lags behind the expansion of the space barrier, creating a non-linear trend. Overall, these findings emphasize that while smaller particles exhibit a predictable, linear force-size relationship, larger particles demonstrate complex capillary interactions that require further investigation to fully elucidate the force trend at greater sizes.

Conclusion

In conclusion, our molecular dynamics simulations have provided comprehensive insights into the wetting behavior and capillary force distribution in nanosuspension droplets composed of liquid Pb with embedded Cu particles on Cu substrates. The study revealed that particle size plays a pivotal role in influencing the kinetics of droplet spreading and the associated capillary forces at the contact line. Larger particles were found to modify the wetting front more substantially, exhibiting non-linear trends in force interactions due to the emergence of space barriers and variable interaction areas. The observation of both pinning and depinning phenomena illustrates how particle-induced changes impact the motion and stability of the contact line, suggesting critical thresholds for particle influence based on size and placement.

The intricate behaviors uncovered include a transition region where the rate of force increase becomes irregular, highlighting the complexities of nanoparticle interactions with liquid fronts. This behavior suggests that beyond a certain particle size, there are diminishing returns or even inhibitory effects on the spreading process due to structural constraints and altered interaction dynamics. These findings underscore the necessity of considering particle distribution and morphology when designing nano-suspensions for applications requiring controlled wetting and spreading properties.

Our work advances the fundamental understanding of how nanoparticle characteristics affect wetting and capillary forces at the nanoscale, offering valuable implications for fields such as material processing, nanofabrication, and microfluidic device design. The non-linear relationship between particle size and capillary force behavior underscores the importance of precise particle engineering to optimize spreading and adhesion in industrial applications. Future research should explore the effects of varying particle compositions and interfacial chemistries to expand on these findings and develop tailored approaches for specific manufacturing needs. This study lays the groundwork for bridging molecular-level observations with practical applications, fostering innovations in surface engineering and nanoparticle-based technologies.

Conflict of Interest

The author(s) declared no potential conflicts of interest with respect to the research, authorship, and/or publication of this article.

References

1. Young T. "An essay on the cohesion of Fluids". Philosophical Transactions of the Royal Society of London 95 (1805): 65-87.
2. de Gennes PG. "Wetting: Statics and dynamics". Reviews of Modern Physics 57.3 (1985): 827-863.
3. D Bonn., et al. "Wetting and spreading". Rev. Mod. Phys 81.2 (2009): 739-805.
4. Kumar A, Zhang X and Liang XJ. "Gold nanoparticles: Emerging paradigm for targeted drug delivery system". Biotechnology Advances 31.5 (2013): 593-606.
5. Wang FC and Wu HA. "Enhanced oil droplet detachment from solid surfaces in charged nanoparticle suspensions". Soft Matter 9.33 (2013): 7974.
6. Tang J and Sargent EH. "Infrared colloidal quantum dots for photovoltaics: Fundamentals and recent progress". Advanced Materials 23.1 (2010): 12-29.
7. Lin Y., et al. "Nanoparticle Assembly and Transport at liquid-liquid interfaces". Science 299.5604 (2003): 226-229.
8. Trantum JR, Wright DW and Haselton FR. "Biomarker-mediated disruption of coffee-ring formation as a low resource diagnostic indicator". Langmuir 28.4 (2012): 2187-93.
9. Wen JT, Ho C-M and Lillehoj PB. "Coffee Ring Apt sensor for rapid protein detection". Langmuir 29.26 (2013): 8440-8446.
10. Brutin D., et al. "Pattern formation in drying drops of blood". Journal of Fluid Mechanics 667 (2010): 85-95.
11. Kim JY., et al. "Crack Formation and prevention in Colloidal drops". Scientific Reports 5 (2015): 13166.
12. Emile J and Tabuteau H. "Effect of the initial particle volume fraction on the structure of a drying colloidal deposit". Colloids and Surfaces A: Physicochemical and Engineering Aspects 511 (2016): 201-211.
13. Ghosh UU., et al. "Contact line dynamics during the evaporation of extended colloidal thin films: Influence of liquid polarity and particle size". Langmuir 32.48 (2016): 12790-12798.
14. Sefiane K, Skilling J and MacGillivray J. "Contact line motion and dynamic wetting of Nanofluid Solutions". Advances in Colloid and Interface Science 138.2 (2008): 101-120.
15. Weon BM and Je JH. "Self-pinning by colloids confined at a contact line". Physical Review Letters 110.2 (2013).
16. Chhasatia VH and Sun Y. "Interaction of bi-dispersed particles with contact line in an evaporating colloidal drop". Soft Matter 7.21 (2011): 10135.
17. Webb EB, Grest GS and Heine DR. "Precursor film controlled wetting of Pb on Cu". Physical Review Letters 91.23 (2003).
18. Foiles SM, Baskes MI and Daw MS. "Embedded-atom-method functions for the FCC metals Cu, Ag, Au, Ni, pd, pt, and their alloys". Physical Review B 33.12 (1986): 7983-7991.
19. Hoyt JJ., et al. "An embedded atom method interatomic potential for the Cu-Pb system". Modelling and Simulation in Materials Science and Engineering 11.3 (2003): 287-299.
20. Lim H, Ong C and Ercolessi F. "Stability of face-centered cubic and icosahedral lead clusters". Surface Science 269-270 (1992): 1109-1115.
21. Shi B and Webb EB. "Self-pinning of a nanosuspension droplet: Molecular dynamics simulations". Physical Review E 94.1-1 (2016): 012614.

Volume 8 Issue 2 February 2025
© All rights are reserved by Baiou Shi., et al.